PAPER

Check for updates

Promotional effect of lanthana on the high-temperature thermal stability of Pt/TiO$_2$ sulfur-resistant diesel oxidation catalysts†

Zhengzheng Yang, [*a] Na Zhang,[a] Yi Cao,[b] Yunxiang Li,[a] Yunwen Liao,[a] Youping Li,[a] Maochu Gong[bc] and Yaoqiang Chen*[bc]

In order to efficiently remove diesel exhaust pollutants during long-term application under high temperature conditions, enhancing the thermal stability of catalysts is essential. Here, lanthana was introduced into a TiO$_2$ sulfur-resistant support *via* co-precipitation, and then a Pt/TiO$_2$–La$_2$O$_3$ diesel oxidation catalyst (DOC) was prepared using the impregnation method. The SO$_2$ uptake and EDX results indicate that the La$_2$O$_3$-doped Pt/TiO$_2$–La$_2$O$_3$ catalyst displays superior sulfur resistance compared to the commercial Pt/Al$_2$O$_3$ and Pt–Pd/CeO$_2$–ZrO$_2$–Al$_2$O$_3$ DOC catalysts. Catalytic performance measurements showed that the as-prepared Pt/TiO$_2$–La$_2$O$_3$ catalyst exhibited significantly better activity than Pt/TiO$_2$ after high-temperature thermal aging and simulative 160 000 km vehicle aging. X-ray diffraction (XRD), X-ray photoelectron spectroscopy (XPS) and N$_2$ adsorption–desorption results suggest that some of the La^{3+} dopant ions migrated to the grain boundary of the TiO$_2$ crystal and other La^{3+} ions replaced Ti^{4+} ionic sites to form Ti–O–La bands, which impeded the crystal growth and phase transition of TiO$_2$, and hence mitigated the destruction of the porous texture of TiO$_2$. Transmission electron microscopy (TEM) and scanning electron microscopy (SEM) observations further demonstrate that the introduction of lanthana into TiO$_2$ suppressed Pt particle agglomeration and catalyst particle sintering, consequently enhancing the thermal stability of the Pt/TiO$_2$–La$_2$O$_3$ catalyst. Thus, this work shows that lanthana can play an extremely important role in improving the structural and textural stability of TiO$_2$ and stabilizing the surface-active component of the Pt/TiO$_2$ DOC catalyst, hence enhancing the high-temperature aging resistance.

1. Introduction

Diesel engines are widely applied due to their robustness and high fuel efficiency. However, hazardous substances from diesel exhausts such as carbon monoxide (CO), unburned hydrocarbons (HCs), various oxides of nitrogen (NO$_x$) and particulate matter (PM) must be effectively removed.[1,2] In recent years, an integrated exhaust after-treatment system, containing a diesel oxidation catalyst (DOC) and a catalyzed diesel particulate filter with selective catalytic reduction, has been widely utilized for purifying diesel exhausts.[3,4] The functions of the DOC in the after-treatment system are removing CO, HCs, and the soluble organic fraction (SOF), and oxidizing NO to NO$_2$.

[a]College of Environmental Science and Engineering, China West Normal University, Nanchong 637009, Sichuan, China. E-mail: zyang@cwnu.edu.cn; Fax: +86 817 2568646; Tel: +86 817 2568646

[b]Key Laboratory of Green Chemistry & Technology of the Ministry of Education, College of Chemistry, Sichuan University, Chengdu 610064, Sichuan, China. E-mail: nic7501@scu.edu.cn; Fax: +86 28 85418451; Tel: +86 28 85418451

[c]Sichuan Provincial Vehicular Exhaust Gases Abatement Engineering Technology Center, Chengdu 610064, Sichuan, China

† Electronic supplementary information (ESI) available. See DOI: 10.1039/c7ra00582b

Noteworthily, the sulfur poisoning resistibility of the DOC is a significant and non-ignorable element,[5–7] because the sulfur content of commercial diesel fuels in developing countries is extremely high.[8,9] Moreover, even with the introduction of ultra-low sulfur diesel (ULSD) fuels, sulfur poisoning still remains one of the most important factors impacting the reactivity of DOCs.[10,11] This is because even with ULSD, SO$_2$ adsorption/condensation/desorption can still be a problem;[12] and current research[10] implies that the amount of sulfur species accumulated on a DOC catalyst over its lifetime may amount to kilograms. Thus, studies on suppressing sulfur species accumulation on DOC catalysts and enhancing the sulfur poisoning resistibility of DOCs are practical and significant.[12]

To improve the sulfur tolerance of catalysts, TiO$_2$, as a non-sulfating material, has been introduced into vehicle exhaust catalysts and has played a commendable role.[12–15] Furthermore, our previous studies[16–18] have suggested that rare earth element doping can improve the activity and stability while maintaining the sulfur resistibility of TiO$_2$-based DOC catalysts. However, the anatase phase transition and decrease in specific surface area of TiO$_2$ under high temperatures[19,20] result in platinum sintering and catalyst deactivation.[12] In the diesel exhaust after-treatment system, during active DPF regeneration, the DOC bed

temperature rises rapidly (and can reach up to 850 °C);[11,21] additionally, diesel engines working at high loading or fast acceleration may also lead to a sharp rise in exhaust temperature. Thus, it is crucial for the thermal stability of TiO_2-based DOCs to be improved.

Research has proven that the addition of La can efficiently enhance the thermal stability of CeO_2 (ref. 22 and 23) and Al_2O_3.[24,25] In addition, the performance of La-doped TiO_2 materials in photocatalytic reactions has been extensively investigated.[26,27] Cong et al.[28] have recently reported that La^{3+} and N co-doping can enhance the thermal stability of TiO_2 microstructures and improve the photocatalytic activity of TiO_2. Moreover, Gopalan, Sibu and Reddy et al. have reported that lanthana doping is conducive to improving the phase and pore structure stability of TiO_2 at high temperature.[29–31]

However, reports on the effects of lanthana on the porous textural features (i.e. specific surface area and pore volume) of TiO_2-based vehicular emission purification catalysts under high temperature are still scarce. Due to the fact that the porous texture of a vehicular emission purification catalyst is closely related to its catalytic performance,[32,33] it is essential to improve the porous texture and high-temperature resistibility of TiO_2. Considering all of this, the effects of lanthana in enhancing the porous texture and high-temperature aging resistance of TiO_2-based sulfur-resistant diesel oxidation catalysts were investigated in this work.

2.   Experimental

2.1   Materials

Ammonium hydroxide, $TiOSO_4 \cdot 2H_2O$, and $La(NO_3)_3 \cdot 6H_2O$ were purchased from Chengdu Kelong Chemical Reagent Factory (China), $(EA)_2Pt(OH)_6$ solution (12.15% Pt w/w) was purchased from Heraeus, and all the chemicals were of analytical grade and used without further purification.

2.2   Catalyst synthesis

The TiO_2–La_2O_3 support was synthesized by co-precipitation with a molar ratio of Ti : La = 9 : 1, which is the optimal ratio according to our previous related work.[17,18] The desired mixed solutions of $TiOSO_4 \cdot 2H_2O$ and $La(NO_3)_3 \cdot 6H_2O$ were slowly added into $NH_3 \cdot H_2O$ solution under vigorous stirring, and then the precipitate was filtered and washed many times. After drying overnight and calcining at 500 °C for 3 h under airflow, the TiO_2–La_2O_3 support was obtained.

The Pt/TiO_2–La_2O_3 catalyst powder was prepared using the incipient impregnation method. $(EA)_2Pt(OH)_6$ solution was impregnated onto the TiO_2–La_2O_3 support with a Pt loading of 1.0 wt%. The resulting Pt/TiO_2–La_2O_3 powder was dried at 120 °C and calcined for 3 h at 500 °C in air, and then the catalyst powder was deposited onto a ceramic honeycomb (400 cells per square inch, 6 mill) with about 120 g L^{-1} of washcoat loading, so as to prepare a monolithic catalyst. The monoliths obtained were dried at 120 °C overnight and calcined for 3 h at 500 °C in air. The Pt/TiO_2 catalyst was synthesized using the same method.

Commercial Pt/Al_2O_3 and $Pt–Pd/CeO_2$–ZrO_2–Al_2O_3 DOC catalysts were supplied by Sichuan provincial vehicular exhaust gases abatement engineering technology center.

The simulative 160 000 km vehicle-aged catalyst, labeled as Pt/TiO_2–La_2O_3(A), was prepared by following ref. 34. Fresh monolithic catalyst was placed in a reactor and aged at 670 °C for 15 h and then at 250 °C for 15 h in the following aging gases: 600 ppm C_3H_6, 1500 ppm CO, 200 ppm NO, 50 ppm SO_2, 5% O_2, 4% CO_2, 8% vapor, and N_2 balance at flow rate of 800 mL min^{-1}. The Pt/TiO_2(A), Pt/Al_2O_3(A) and $Pt–Pd/CeO_2$–ZrO_2–Al_2O_3(A) catalysts were obtained using the same method.

2.3   Catalytic performance measurements

The activities of the catalysts were tested on a multiple fixed bed continuous flow reactor. The monolith was placed in a quartz tube reactor with an electric heater. The simulative diesel exhaust gases[35] contained a mixture of 1000 ppm CO, 330 ppm C_3H_6, 200 ppm NO, 50 ppm SO_2, 8% CO_2, 7% vapor, 10% O_2, and N_2 balance at a gas space velocity of 60 000 h^{-1}, and were controlled by mass flow controllers.

The inlet gas temperature was measured by a K-thermocouple which was fixed 20 mm in front of the monolith to avoid the effect of oxidation reactions (exothermic). The catalyst bed temperature was measured by another 0.5 mm K-thermocouple which was placed in the middle of one of the center channels inside the monolith catalyst. The outlet CO was detected using an FGA-4100 automotive emission analyzer (Foshan Analytical Instrument Co., Ltd., China), and C_3H_6 was analyzed with a GC2000II online gas chromatograph (Shanghai Analysis Instruments, China) using a flame ionization detector (FID).

2.4   Catalyst characterization

SO_2 uptake testing was conducted as reported in ref. 36 and implemented on a HCT-2 (Henven Instruments, China) thermogravimetric analyzer (TGA). The samples (15 mg) were pretreated in a 35 mL min^{-1} flow of N_2 for 5 h at 300 °C. Then, a flow of 43 mL min^{-1} SO_2(0.05 vol%)–N_2 and 31 mL min^{-1} O_2(15.0 vol%)–N_2 was introduced at 300 °C for 4 h. The accumulation of sulfur species was defined as the percentage of mass gained.

CO chemisorption was performed in a quartz tube reactor at room temperature. About 0.15 g of sample was reduced in a hydrogen flow (H_2, 99.999%) of 50 mL min^{-1} at 500 °C and exposed for 2 h. After cooling to room temperature in the same reducing stream, helium (He, 99.999%) was flowed through the sample for 10 min, and then the Pt dispersion of the sample was determined by CO chemisorption. Because both linearly bound and bridge-bound CO existed on the Pt catalyst, a factor of 0.8 CO/Pt was used to calculate the concentration of surface Pt atoms.[37]

X-ray diffraction (XRD) patterns of the samples were obtained by power X-ray diffraction on a DX-1000 diffractometer (Dandong Fangyuan Instrument Co. Ltd., China) using Cu Kα radiation.

X-ray photoelectron spectroscopy (XPS) data were acquired using a Kratos XSAM 800 spectrometer (Kratos Analytic Inc.)

with Al Kα radiation, and the C 1s binding energy (BE, 284.8 eV) was used to calibrate the binding energy shifts of the samples.

Nitrogen adsorption–desorption isotherms were obtained on a QUADRASORB SI automated surface area and pore size analyzer (Quantachrome Instruments). The specific surface area and pore size were calculated using the BET and BJH method, respectively.

TEM images were acquired on a Tecnai G^2 F20 (E. A. Fischione Instruments Inc., USA) transmission electron microscope (TEM).

The surface morphologies of the catalysts were observed using a S-4800 (Hitachi Ltd.) scanning electron microscope (SEM), and the sulfur content of the aged catalysts was analyzed using an IE-250 (Oxford Instruments) energy dispersive X-ray (EDX) spectrometer.

3. Results and discussion

3.1 Sulfur resistibility

The sulfur resistibility of the catalysts was tested using SO_2 uptake testing. As shown in Fig. 1, following exposure to SO_2 and O_2, the weight of the as-prepared Pt/TiO_2 and Pt/TiO_2–

Fig. 1 SO_2 uptake of the as-prepared Pt/TiO_2 and Pt/TiO_2–La_2O_3, and commercial Pt/Al_2O_3 and Pt–Pd/CeO_2–ZrO_2–Al_2O_3 catalysts.

La_2O_3 catalyst samples increased with time; after about 3 h, the weight changing trend of the samples began to level-off. The final weight increments of the Pt/TiO_2 and Pt/TiO_2–La_2O_3 samples were about 1.80 wt% and 2.46 wt%, respectively. In the same SO_2 uptake experiment, the total weight increments of the current commercial Pt/Al_2O_3 and Pt–Pd/CeO_2–ZrO_2–Al_2O_3 DOC catalysts were about 5.66 wt% and 4.73 wt%, respectively. The normalized sulfur uptake was calculated using the following equation:[36]

$$\text{Normalized sulfur uptake } (\mu g\ m^{-2}) = \frac{\text{sulfur content (wt\%)}}{100 \times \text{surface area (m}^2)}$$

where the surface area is the BET surface area of the sample.

The calculated results are listed in Table 1. The normalized sulfur uptakes of the Pt/TiO_2 and Pt/TiO_2–La_2O_3 samples were about 194 μg m^{-2} and 191 μg m^{-2}, respectively; for the commercial Pt/Al_2O_3 and Pt–Pd/CeO_2–ZrO_2–Al_2O_3 DOC catalysts, the values were about 306 μg m^{-2} and 230 μg m^{-2}, respectively. This indicates that compared with the current commercial Pt/Al_2O_3 and Pt–Pd/CeO_2–ZrO_2–Al_2O_3 DOC catalysts, the TiO_2-based catalysts (both Pt/TiO_2 and Pt/TiO_2–La_2O_3) did not heavily accumulate sulfur species, and hence the TiO_2-based catalysts displayed superior sulfur resistibility. This is because the non-sulfating material TiO_2 exhibits low SO_2 adsorption, and hence suppresses sulfate formation.[12,38] Moreover, the doping of La into TiO_2 had essentially no effect on the naturally excellent sulfur resistance of the Pt/TiO_2 catalyst.

Meanwhile, according to the EDX testing results (Table 1), the amount of sulfur accumulated on the simulative 160 000 km vehicle-aged $Pt/TiO_2(A)$ and Pt/TiO_2–$La_2O_3(A)$ catalysts was about 1.34 wt% and 1.85 wt%, respectively, while the values for the commercial $Pt/Al_2O_3(A)$ and Pt–Pd/CeO_2–ZrO_2–$Al_2O_3(A)$ DOC catalysts were about 5.79 wt% and 4.40 wt%, respectively. The normalized sulfur uptake values calculated from the EDX results also showed the same trend, which implies that compared with the current commercial Pt/Al_2O_3 and Pt–Pd/CeO_2–ZrO_2–Al_2O_3 DOC catalysts, the as-prepared Pt/TiO_2 and Pt/TiO_2–La_2O_3 catalysts exhibit obviously reduced sulfur accumulation under long-term exposure to diesel exhaust conditions. Additionally, the catalytic activity measurements show that both the as-prepared Pt/TiO_2 and Pt/TiO_2–La_2O_3, and the commercial Pt/Al_2O_3 and Pt–Pd/CeO_2–ZrO_2–Al_2O_3 DOC catalysts displayed good purifying properties for diesel exhaust CO and C_3H_6; all the mentioned
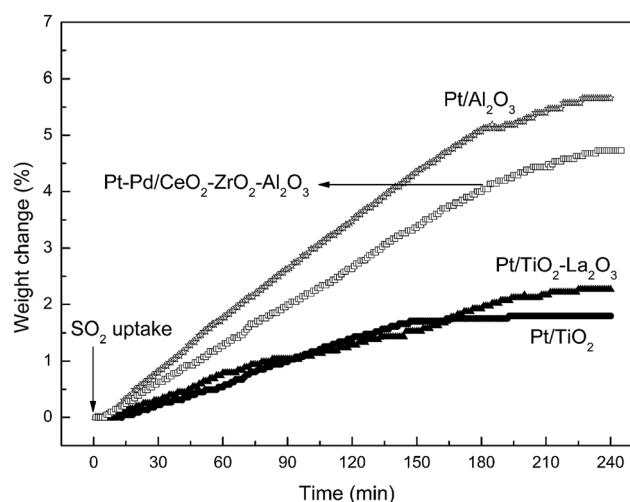
Table 1 Sulfur accumulation and normalized sulfur uptake over the Pt/TiO_2, Pt/TiO_2–La_2O_3, and commercial Pt/Al_2O_3 and Pt–Pd/CeO_2–ZrO_2–Al_2O_3 DOC catalysts

Sample	Surface area/(m^2)	Sulfur content (wt%)		Normalized sulfur uptake (μg m^{-2})	
		SO_2 uptake	EDX[a]	SO_2 uptake	EDX[a]
Pt/TiO_2	93	1.80	1.34	194	144
Pt/TiO_2–La_2O_3	129	2.46	1.85	191	143
Pt/Al_2O_3	185	5.66	5.79	306	313
Pt–Pd/CeO_2–ZrO_2–Al_2O_3	206	4.73	4.40	230	214

[a] EDX results were obtained by detecting the simulative 160 000 km vehicle-aged samples.

catalysts can completely purify diesel CO and C_3H_6 below 230 °C (ESI, Fig. 1†).

Because sulfur accumulation on catalysts leads to sulfur poisoning of the catalyst and hence activity degradation, our previous work verified that the commercial Pt/Al_2O_3 and Pt–Pd/CeO_2–ZrO_2–Al_2O_3 DOC catalysts were significantly deactivated due to the accumulation of sulfur on the catalyst surface, but the activity degradation of TiO_2-based catalysts resulting from sulfur poisoning was very slight.[17] Thus, it can be suggested that compared to the current commercial Pt/Al_2O_3 and Pt–Pd/CeO_2–ZrO_2–Al_2O_3 DOC catalysts, the TiO_2-based catalysts (Pt/TiO_2 and Pt/TiO_2–La_2O_3) displayed superior sulfur resistibility, which is beneficial for maintaining catalytic activity during long-term use under SO_2-containing diesel exhaust conditions.

3.2 Catalytic activity and thermal stability

3.2.1 Effects of lanthana modification. Fig. 2 shows the catalytic activities of CO and C_3H_6 oxidation on the fresh and thermally aged Pt/TiO_2 and Pt/TiO_2–La_2O_3 catalysts. It can be seen that the catalytic performances of both the Pt/TiO_2 and Pt/TiO_2–La_2O_3 catalysts are decreased after 3 h of thermal treatment at 750 °C; however, modification with La significantly alleviated the reactivity decrease of the Pt/TiO_2–La_2O_3 catalyst. For the CO oxidation reaction (Fig. 2a), 3 h of thermal treatment at 750 °C lead to an 11 °C increase in the light-off temperature (T_{50}, the temperature when the conversion of the reactant reaches 50%) on the Pt/TiO_2 catalyst; the T_{50} increment of the Pt/TiO_2–La_2O_3 catalyst resulting from aging at 750 °C is negligible (less than 2 °C). The same trend was also observed for the C_3H_6 combustion reaction (Fig. 2b), which demonstrates that La modification obviously mitigated the activity decrease of Pt/TiO_2 resulting from high-temperature treatment; that is, La doping can effectively enhance the thermo-stability of the Pt/TiO_2 catalyst.

Furthermore, the Pt/TiO_2–La_2O_3 catalyst shows significantly better catalytic performance than the Pt/TiO_2 catalyst, both after 3 h of thermal aging at 850 °C and after simulative 160 000 km vehicle aging (ESI, Fig. 2 and 3†). The CO and C_3H_6 T_{50} values of Pt/TiO_2–La_2O_3(850), the sample treated at 850 °C for 3 h, are 221 °C and 236 °C, respectively; for Pt/TiO_2(850) the values are 232 °C and 240 °C, respectively (ESI, Fig. 2†). The 160 000 km vehicle-aged sample Pt/TiO_2–La_2O_3(A) shows CO and C_3H_6 light-off temperatures of 210 °C and 218 °C, respectively; the CO and C_3H_6 T_{50} values of Pt/TiO_2(A) are 219 °C and 231 °C, respectively (ESI, Fig. 3†). It can be inferred that La doping results in an improvement in high-temperature resistance and long-term use durability. Additionally, it was proved that yttria-modified Pt/TiO_2–YO_x catalysts exhibited excellent low temperature activity and stability in our previous work,[17] and the high-temperature resistibility of the Pt/TiO_2–YO_x catalyst was compared with that of the Pt/TiO_2–La_2O_3 catalyst (ESI, Fig. 4†). It can be seen that the Pt/TiO_2–YO_x catalyst showed the best low temperature activity for CO and C_3H_6 oxidation; however, after 3 h of thermal aging at 750 °C, the Pt/TiO_2–La_2O_3 catalyst displayed obviously better activity than Pt/TiO_2–YO_x, and after thermal aging at 850 °C for 3 h, Pt/TiO_2–La_2O_3 still exhibited better activity than
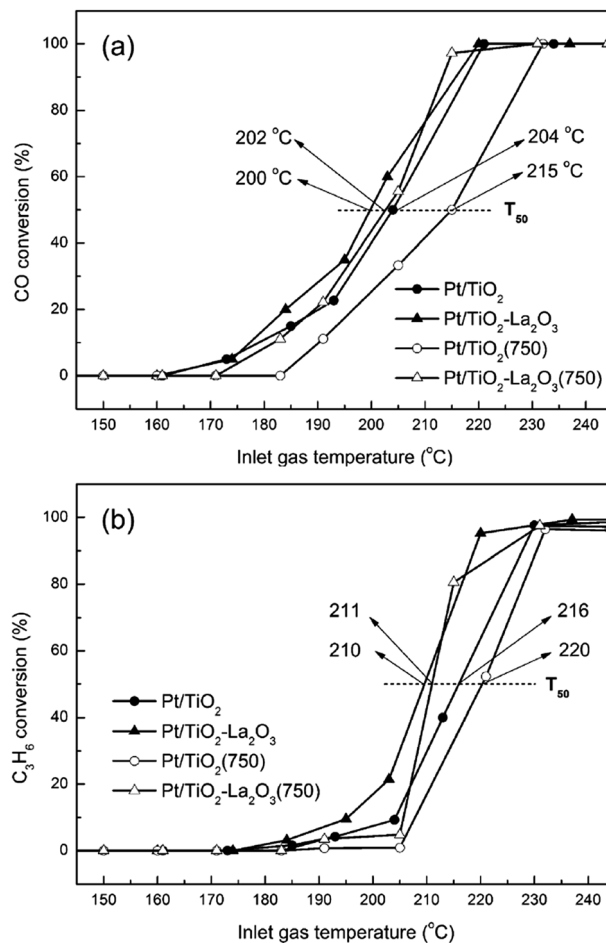

Fig. 2 The CO (a) and C_3H_6 (b) oxidation conversion over Pt/TiO_2, Pt/TiO_2–La_2O_3, Pt/TiO_2(750) and Pt/TiO_2–La_2O_3(750) catalysts. Reaction conditions: C_3H_6: 330 ppm, CO: 1000 ppm, NO: 200 ppm, O_2: 10%, CO_2: 8%, vapor: 7%, SO_2: 50 ppm, N_2: balance, GHSV = 60 000 h^{-1}. All catalysts were pre-treated at 500 °C for 3 h under the reaction atmosphere.

the Pt/TiO_2–YO_x catalyst. This suggests that the high-temperature resistibility of the lanthana-modified Pt/TiO_2–La_2O_3 catalyst is superior to that of the yttria-modified Pt/TiO_2 catalyst.

To clearly investigate the effects of La modification on the DOC reactivity after high-temperature treatment, the global reaction rates of both catalysts before and after 3 h of thermal treatment at 750 °C were determined. The calculated reaction rate results are listed in Table 2. It can be seen that the reaction rate of the Pt/TiO_2 catalyst for CO oxidation is 4.20×10^{-6} mol g^{-1} s^{-1}, and the value reduces to 2.59×10^{-6} mol g^{-1} s^{-1} after thermal treatment at 750 °C for 3 h, which indicates that high-temperature treatment leads to a 40% reaction rate decrease of Pt/TiO_2 for CO oxidation. For the Pt/TiO_2–La_2O_3 catalyst, the catalytic activity decrease following the same thermal treatment could be ignored, because it was within the limit of measurement error (from 4.74×10^{-6} mol g^{-1} s^{-1} to 4.75×10^{-6} mol g^{-1} s^{-1}). For C_3H_6 combustion, 3 h of high-temperature treatment at 750 °C resulted in a 43% decrease (from 6.09×10^{-7} mol g^{-1} s^{-1} to 3.49×10^{-7} mol g^{-1} s^{-1}) in the

Table 2 CO and C_3H_6 reaction rates at 210 °C over the Pt/TiO$_2$, Pt/TiO$_2$–La$_2$O$_3$, Pt/TiO$_2$(750) and Pt/TiO$_2$–La$_2$O$_3$(750) catalysts

	Reaction rate (mol g^{-1} s^{-1})	
Catalyst	CO + O$_2$	C$_3$H$_6$ + O$_2$
Pt/TiO$_2$	4.20×10^{-6}	6.09×10^{-7}
Pt/TiO$_2$(750)	2.59×10^{-6}	3.49×10^{-7}
Pt/TiO$_2$–La$_2$O$_3$	4.74×10^{-6}	10.6×10^{-7}
Pt/TiO$_2$–La$_2$O$_3$(750)	4.75×10^{-6}	8.74×10^{-7}

global reaction rate of the Pt/TiO$_2$ catalyst at 210 °C, while the decrease of the reaction rate of the Pt/TiO$_2$–La$_2$O$_3$ catalyst resulting from the high-temperature treatment is negligible (from 10.6×10^{-7} mol g^{-1} s^{-1} to 8.74×10^{-7} mol g^{-1} s^{-1}). The activation energies of CO and C$_3$H$_6$ oxidation were not calculated because the presence of mixed gases (CO, C$_3$H$_6$, NO *etc.*) under simulative diesel exhaust conditions may affect the kinetic parameters of CO and C$_3$H$_6$ oxidation.[17,39] Based on the above results, it can be suggested that the modification of the Pt/TiO$_2$ catalyst with La significantly mitigated the decrease in DOC reactivity resulting from high-temperature treatment, which in essence indicates that La doping can improve the thermo-stability of the Pt/TiO$_2$ catalyst.

3.2.2 Effects of high-temperature treatment. The relationship between the treatment temperature and the reaction rate at 210 °C for both of the catalysts is shown in Fig. 3. It is clear that the DOC reactivity of both the Pt/TiO$_2$ and Pt/TiO$_2$–La$_2$O$_3$ catalyst was not affected by 3 h of thermal treatment at 650 °C, which implies that the activity of both the catalysts could be maintained under the normal working conditions of a diesel engine. After thermal treated at 750 °C for 3 h, the CO and C$_3$H$_6$ catalytic performance of the Pt/TiO$_2$(750) catalyst was reduced by about 40% compared to the fresh Pt/TiO$_2$ catalyst, whereas the reactivity of Pt/TiO$_2$–La$_2$O$_3$(750) was almost not reduced; that is, an ultra-high exhaust temperature resulting from DPF regeneration or the diesel engine working under extreme conditions (such as ultra-high loading or fast acceleration *etc.*)

would lead to the deactivation of the Pt/TiO$_2$ catalyst, but La doping can efficiently restrain the reactivity loss and enhance the thermal stability. The Pt/TiO$_2$–La$_2$O$_3$ catalyst was not obviously deactivated until the sample endured 3 h of baking at 850 °C. In order to investigate the effects of La in the Pt/TiO$_2$ catalyst, several characterization techniques were carried out.

3.3 Catalyst characterization

3.3.1 XRD analysis. Fig. 4 shows the XRD patterns of the TiO$_2$ and TiO$_2$–La$_2$O$_3$ supports at different temperatures. Typical anatase structure peaks are observed in the TiO$_2$ sample calcined at 500 °C, with a crystallite size of about 9.3 nm. As the temperature increased to 700 °C, a phase transition from anatase to rutile occurred; the ratio of rutile was about 14.3%, and the anatase crystallite size increased to 18 nm. When the temperature reaches 800 or 900 °C, the phase of TiO$_2$ is rutile with an average crystallite size of 33 or 39 nm. For all the La$_2$O$_3$-modified TiO$_2$ samples, no XRD characteristic peaks due to the crystalline La$_2$O$_3$ phase were observed; this observation indicates that La$_2$O$_3$ does not form complete crystals, and the La$_2$O$_3$ may be in a highly dispersed state or the La$_2$O$_3$ crystallites formed may be smaller than the detection ability of the XRD technique. TiO$_2$–La$_2$O$_3$ is mainly amorphous after calcining at 500 °C. Anatase structure peaks are observed in the TiO$_2$–La$_2$O$_3$ sample calcined at 700 °C, with a crystallite size of about 13 nm, and for the TiO$_2$–La$_2$O$_3$ sample calcined at 800 °C, the phase is still anatase with a crystallite size of 18 nm. The characteristic peaks of rutile are not observed until the temperature reaches up to 900 °C where the rutile characteristic peaks are weak, and the anatase crystallite size of the TiO$_2$–La$_2$O$_3$ sample calcined at 900 °C is about 30 nm. It can be seen that La$_2$O$_3$ modification retards the anatase–rutile phase transformation and postpones the crystal growth of TiO$_2$ under high temperature, thus stabilizing the structural properties of TiO$_2$. Moreover, the stabilization of the TiO$_2$ crystals by La$_2$O$_3$ is favorable for preventing the destruction of the texture of the TiO$_2$-based supports,[19,20,40]
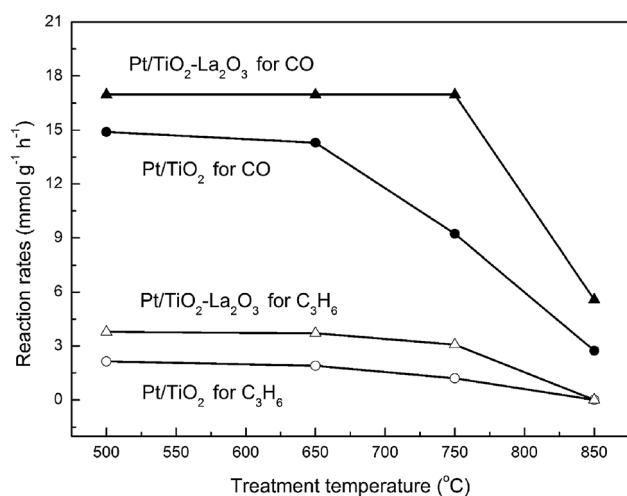

Fig. 3 CO and C$_3$H$_6$ reaction rates at 210 °C over the Pt/TiO$_2$ and Pt/TiO$_2$–La$_2$O$_3$ catalysts after 3 h of treatment at different temperatures.
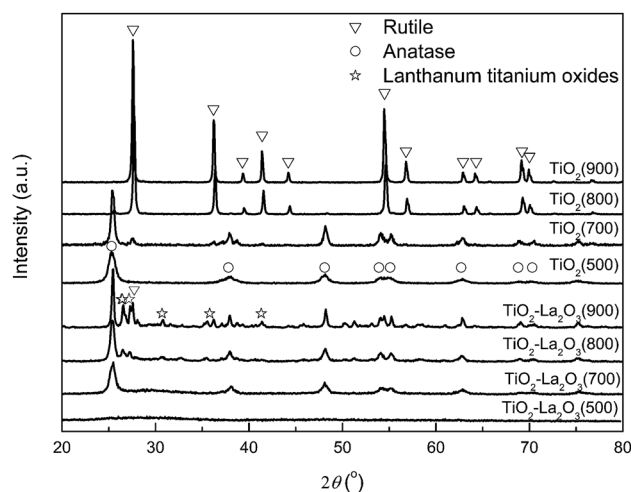

Fig. 4 XRD patterns of the TiO$_2$ and TiO$_2$–La$_2$O$_3$ supports after 3 h of treatment at different temperatures.

and enhancing the high-temperature resistance of the TiO_2-based catalyst.

Because the ionic radius of La^{3+} (0.1016 nm) is between that of Ti^{4+} (0.068 nm) and O^{2-} (0.132 nm),[30,41] the La^{3+} ions should either replace the Ti^{4+} site or migrate to the grain boundary.[30] Thus, the stabilization of La_2O_3 in the TiO_2 crystal can be partly attributed to the segregation of lanthana dopant ions at the interstitial, which can inhibit the grain growth of TiO_2 by increasing the diffusion barrier at the titania–titania grain contacts and restricting the direct contact of the grains.[30,42]

Besides the interstitial La_2O_3 segregation, the formation of Ti–O–La bands at the interface, resulting from some of the La^{3+} ions replacing some of the Ti^{4+} ionic sites, is another reason why La_2O_3 shows a stabilizing effect in TiO_2.[28,43–45] Reddy, Sibu and Xu *et al.* have proven that Ti–O–La bands are formed in La_2O_3-doped TiO_2 mixed oxides.[30,46,47] To further confirm the formation of Ti–O–La bands in the TiO_2–La_2O_3 compound in this work, XPS was employed.

3.3.2 XPS. The XPS spectra of the O 1s region of the as-prepared Pt/TiO_2 and Pt/TiO_2–La_2O_3 catalysts are provided in Fig. 5. Two peaks are observed for the Pt/TiO_2 sample; the peak with a binding energy of 530.0 eV is characteristic of lattice oxygen, and that with a binding energy of about 532.6 eV can be assigned to surface adsorbed oxygen.[48–50] For the Pt/TiO_2–La_2O_3 catalyst, the characteristic peak of lattice oxygen is located at 529.7 eV, which is obviously shifted to a lower binding energy (decreasing by 0.3 eV); the peak for surface adsorbed oxygen is also located at 532.6 eV and the peak at 531.0 eV can be attributed to the contribution of chemisorbed oxygen or defect oxygen,[49,50] which may result from the lattice oxygen separation of La_2O_3.[51,52]

The XPS binding energy values of the Ti $2p_{3/2}$ and La $3d_{5/2}$ regions are listed in Table 3. The standard binding energy values of Ti $2p_{3/2}$ in TiO_2 and La $3d_{5/2}$ in La_2O_3 are 458.5 eV and 834.8 eV, respectively.[53] The binding energy of Ti in the Pt/TiO_2 catalyst is 458.5 eV, which is characteristic of TiO_2 (Ti^{4+}) species, and this value is the same that for standard TiO_2. The binding energy of Ti in the Pt/TiO_2–La_2O_3 catalyst is 458.2 eV, which is

Table 3 Ti 2p and La 3d XPS parameters of the Pt/TiO_2 and Pt/TiO_2–La_2O_3 catalysts

Catalyst	Binding energy (eV)	
	Ti $2p_{3/2}$	La $3d_{5/2}$
Pt/TiO_2	458.5	—
Pt/TiO_2–La_2O_3	458.2	834.8
TiO_2	458.5 (ref. 53)	—
La_2O_3	—	834.9 (ref. 53)

obviously shifted to a lower energy than the value for standard TiO_2; this result indicates that some of the La^{3+} ions replace some of the Ti^{4+} sites and display a strong interaction with TiO_2. Meanwhile, the binding energy of La in the Pt/TiO_2–La_2O_3 catalyst is 834.8 eV, very close to the standard La_2O_3 value (834.9 eV), which suggests that in addition to the La^{3+} ions replacing the Ti^{4+} sites of TiO_2, a large number of La^{3+} ions in the Pt/TiO_2–La_2O_3 catalyst exist in the form of La_2O_3 species. These La_2O_3 species can act as a segregation agent in the TiO_2–La_2O_3 composite and hence inhibit TiO_2 grain growth by increasing the diffusion barrier and restricting the direct contact of the TiO_2–TiO_2 grains.[30,42]

As presented in Fig. 5 and Table 3, in the Pt/TiO_2–La_2O_3 catalyst, the XPS characteristic binding energy values of both lattice oxygen (O^{2-}) and Ti^{4+} are obviously shifted to lower binding energies, which can be attributed to the formation of Ti–O–La bands.[46] The formation of Ti–O–La bands provides a route for La^{3+} (which is more electropositive) to transfer electrons to O^{2-}, and the increased concentration of electrons can be used to strengthen the bonding between the less electropositive Ti^{4+} ions.[30,46] The increase in the electron density of O^{2-} and Ti^{4+} in the TiO_2–La_2O_3 composite results in the XPS binding energy shifting to lower values. Furthermore, the La^{3+} stabilized Ti–O bonds will in turn defer the phase transformation temperature of anatase-to-rutile, because the anatase-to-rutile phase transition requires the breaking of Ti–O bonds,[30] and the Ti–O bonds enhanced by La^{3+} ions are more difficult to break. Thus, the La_2O_3-stabilized TiO_2 exhibits superior high-temperature thermal stability.

3.3.3 Nitrogen adsorption–desorption. The stabilization of the structural properties of TiO_2 by La_2O_3 doping may enhance the textural stability of the TiO_2–La_2O_3 composite. To determine the texture of each catalyst support, the N_2 adsorption–desorption technique was used. As shown in Fig. 6, both the as-synthesized TiO_2(500) and TiO_2–La_2O_3(500) show distinct H3 and H4 complex hysteresis loops indicating slit pore features.[54,55] When 3 h of thermal treatment at 700 °C was employed, some of the pores in both samples collapsed, but a distinct porous structure was still observed. After calcination at 800 °C for 3 h, which simulated high temperatures in a DOC bed resulting from active DPF regeneration, the TiO_2 support showed no obvious pore characteristics; however, the TiO_2–La_2O_3 support still showed a significant H3 hysteresis loop indicating slit pore features provided by schistous particles,[54,55] until the temperature reached as high as 900 °C.
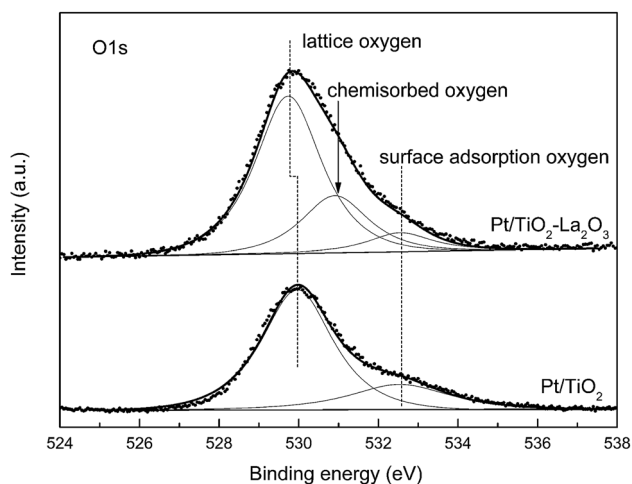

Fig. 5 XPS (O 1s) spectra of the Pt/TiO_2 and Pt/TiO_2–La_2O_3 catalysts.
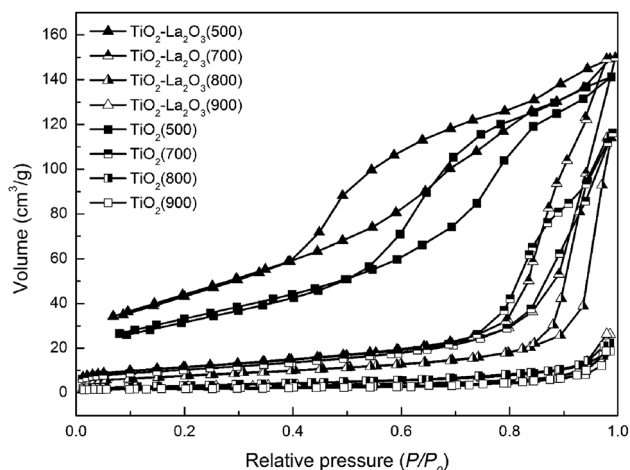
Fig. 6 Nitrogen adsorption–desorption isotherms of the TiO$_2$ and TiO$_2$–La$_2$O$_3$ supports after 3 h of treatment at different temperatures.

The calculated porous parameter results are listed in Table 4. The fresh TiO$_2$(500) and TiO$_2$–La$_2$O$_3$(500) supports show similar textural properties; the specific surface area of TiO$_2$(500) is approximately 98 m^2 g^{-1} with an average pore volume of about 0.22 cm^3 g^{-1}, and the specific surface area and average pore volume of TiO$_2$–La$_2$O$_3$(500) are about 129 m^2 g^{-1} and 0.23 cm^3 g^{-1}, respectively. Thermal treatment at 700 °C for 3 h led to a reduction in the surface area of both samples to near 40 m^2 g^{-1}. When 3 h of thermal treatment at 800 °C was employed, the TiO$_2$(800) sample lost its porous features, and the surface area and pore volume are just 11 m^2 g^{-1} and 0.03 cm^3 g^{-1}, respectively. In contrast, the surface area of La doped-TiO$_2$ is more than 30 m^2 g^{-1}, and in particular the pore volume of TiO$_2$–La$_2$O$_3$(800), 0.18 cm^3 g^{-1}, is similar to that of the fresh sample, which indicates that baking at 800 °C for 3 h did not obviously block the open pores and did not destroy the porous characteristics of the TiO$_2$–La$_2$O$_3$ support. As a result, the embedding of catalyst active components as a result of the texture of the support being destroyed is relieved. It is thus clear that La doping efficiently relieved the high-temperature sintering of TiO$_2$, and maintained the good porous texture of the TiO$_2$–La$_2$O$_3$ support at high temperatures.

In order to further investigate the relationship between the structural properties and textural features of TiO$_2$, the surface

area–crystallite size relationships of both supports after treatment at different temperatures were investigated as shown in Fig. 7. The crystallite size of amorphous TiO$_2$–La$_2$O$_3$(500) was crudely estimated using the unsharp (101) crystal face of anatase, and the crystallite size of TiO$_2$ after calcining at 800 °C and 900 °C was calculated using the rutile crystal faces. It can be found that the surface area of both the TiO$_2$ and TiO$_2$–La$_2$O$_3$ supports declines and the crystallite size increases as the temperature rises. When the crystallite size is smaller than 20 nm, the surface area sharply declines with an increase in temperature; after that, when the crystallite size is larger than 20 nm, the changes in surface area and crystallite size with a rise in temperature tend to be moderate. Note that a surface area of no less than 30 m^2 g^{-1} is required to maintain the catalytic performance of vehicular emissions purification catalysts.[32,56,57] The TiO$_2$ support exhibits a crystallite size of about 20 nm and a surface area of 30 m^2 g^{-1} at about 700 °C, and the La-doped TiO$_2$ shows similar properties after 3 h of treatment at 800 °C, which means that the TiO$_2$-based catalyst can hardly maintain good activity at temperatures higher than 800 °C, but the TiO$_2$–La$_2$O$_3$ catalyst can. That is, La modification can lead to TiO$_2$-based DOCs that retain good reactivity at temperatures higher than 800 °C (the DOC bed temperature during active DPF regeneration). This corollary was confirmed by ESI Fig. 2.†

3.3.4 TEM. Catalyst supports with superior porous textures are advantageous for the dispersion of the active phase and hence improving the catalytic activity.[58–60] The Pt particle sizes of the fresh and simulative vehicle-aged catalysts were observed by TEM. As presented in Fig. 8a and b, the Pt particles on the fresh Pt/TiO$_2$ and Pt/TiO$_2$–La$_2$O$_3$ catalysts are highly and homogeneously dispersed on the surface of the supports, and mimicking 160 000 km of vehicular exhaust aging obviously contributes to the Pt particle sintering of the Pt/TiO$_2$(A) (Fig. 8c) and Pt/TiO$_2$–La$_2$O$_3$(A) (Fig. 8d) catalysts. Based on the Pt particle size statistics obtained from the TEM images, the Pt particle size distributions of the catalysts were acquired and are displayed in Fig. 8e–h. For the Pt/TiO$_2$ catalyst (Fig. 8e), the Pt particle size
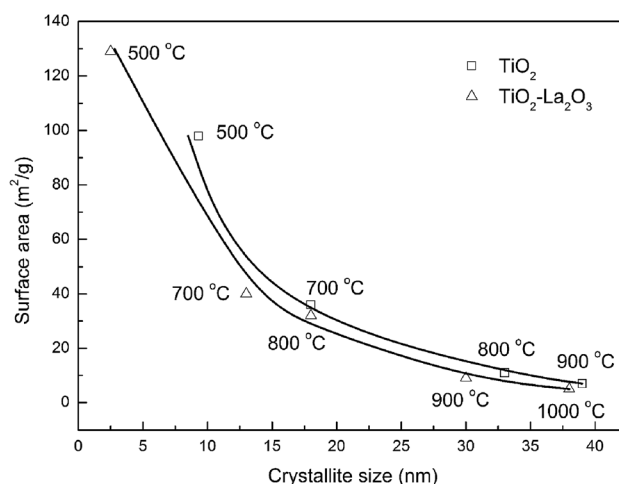
Table 4 Textural properties of the TiO$_2$ and TiO$_2$–La$_2$O$_3$ supports after 3 h of treatment at different temperatures

Sample	Surface area (m^2 g^{-1})	Pore volume (cm^3 g^{-1})
TiO$_2$(500)	98	0.22
TiO$_2$–La$_2$O$_3$(500)	129	0.23
TiO$_2$(700)	36	0.18
TiO$_2$–La$_2$O$_3$(700)	40	0.23
TiO$_2$(800)	11	0.03
TiO$_2$–La$_2$O$_3$(800)	32	0.18
TiO$_2$(900)	7	0.03
TiO$_2$–La$_2$O$_3$(900)	9	0.04

Fig. 7 The surface area–crystallite size relationships of the TiO$_2$ and TiO$_2$–La$_2$O$_3$ supports after 3 h of treatment at different temperatures.

distribution is between 0.73 nm and 3.28 nm with a mean size of 1.57 nm, estimated from over 300 particles from multiple TEM images. The Pt particle mean diameter of the Pt/TiO$_2$–

La$_2$O$_3$ catalyst (Fig. 8f) is about 1.39 nm and the size distribution is in the range of 0.65–3.25 nm (counting more than 300 Pt particles). To observe the Pt particles on the fresh catalysts more
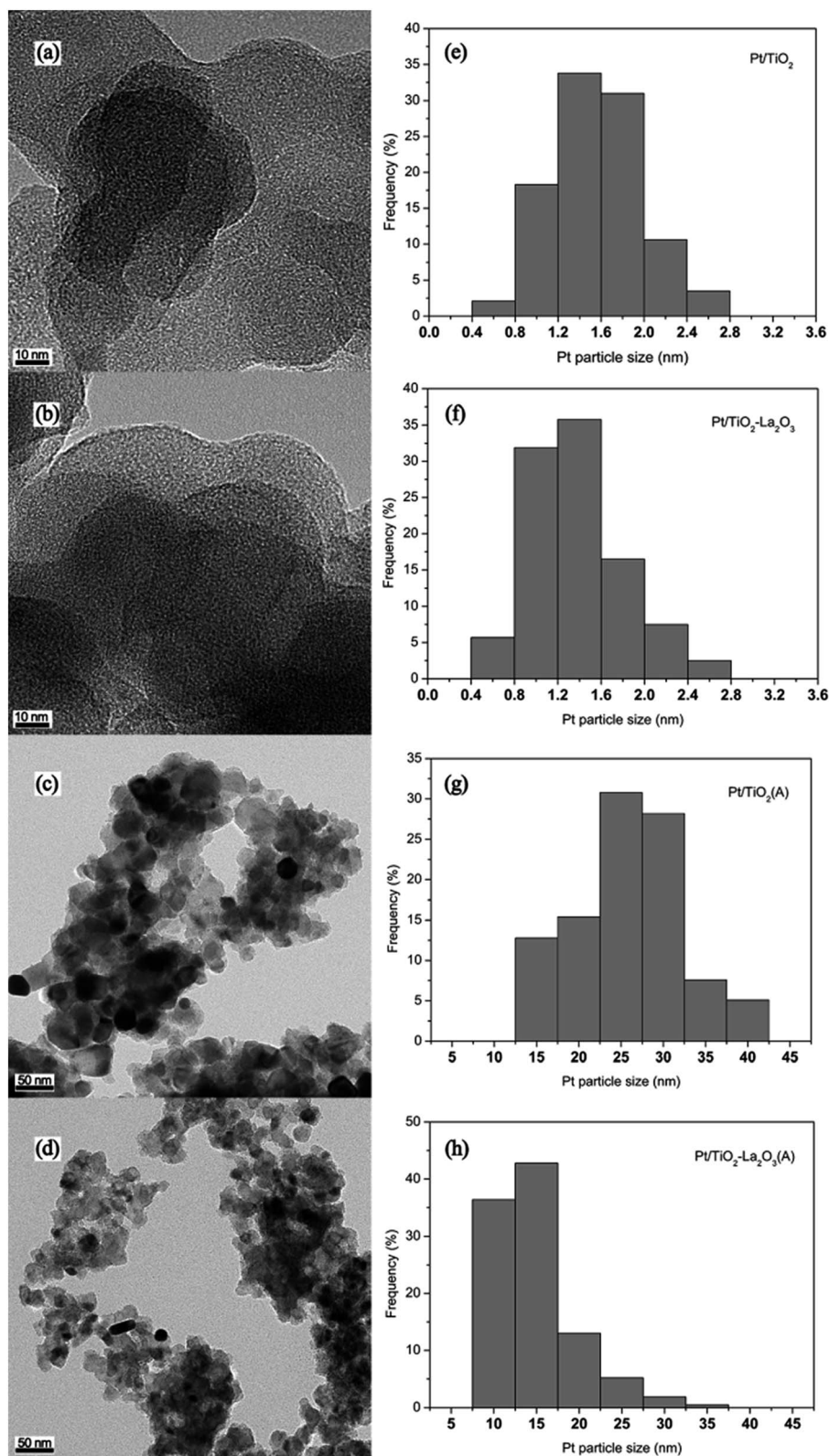

Fig. 8 TEM micrographs of the (a) Pt/TiO$_2$, (b) Pt/TiO$_2$–La$_2$O$_3$, (c) Pt/TiO$_2$(A), and (d) Pt/TiO$_2$–La$_2$O$_3$(A) catalysts, and (e–h) the related size distributions.

Table 5 Pt particle characteristics on the fresh and aged catalysts

Catalyst	Pt mean size (nm)	Pt surface area to volume ratio
Pt/TiO$_2$	1.57	0.71
Pt/TiO$_2$–La$_2$O$_3$	1.39	0.80
Pt/TiO$_2$(A)	25.90	0.043
Pt/TiO$_2$–La$_2$O$_3$(A)	14.78	0.076

Table 6 Pt surface concentration of the fresh and aged catalysts

Catalyst	Pt content (at%)
Pt/TiO$_2$	0.87
Pt/TiO$_2$–La$_2$O$_3$	0.73
Pt/TiO$_2$(A)	0.07
Pt/TiO$_2$–La$_2$O$_3$(A)	0.27

clearly, higher resolution TEM images were acquired and are supplied in Fig. 5 in the ESI.† For the aged catalysts, the mean Pt particle sizes of Pt/TiO$_2$(A) (Fig. 8g) and Pt/TiO$_2$–La$_2$O$_3$(A) (Fig. 8h) are 25.90 nm (in the range of 13.48 nm to 42.66 nm) and 14.78 nm (in the range of 8.26 nm to 36.42 nm), respectively, estimated from about 200 particles from multiple TEM images. Pt particles of smaller size have a better catalytic oxidation activity,[61–63] due to the fact that smaller Pt particles supply a larger surface area to volume ratio and hence exhibit more surface Pt atoms (active phases).[16,64] The Pt surface area to volume ratios of the as-prepared catalysts were estimated using the crude sphere model[16,17] and are displayed in Table 5. It can be seen that the Pt surface area to volume ratio of Pt/TiO$_2$ is 0.72, which is roughly identical to the value (0.80) of the Pt/

TiO$_2$–La$_2$O$_3$ catalyst. However, the surface Pt atomic ratio of the aged Pt/TiO$_2$–La$_2$O$_3$(A) catalyst is about 0.076, which is almost twice as high as the surface Pt ratio (0.043) of the aged Pt/TiO$_2$(A) catalyst. It is thus clear that the Pt particles on both the Pt/TiO$_2$ and Pt/TiO$_2$–La$_2$O$_3$ catalysts are sintered into larger particles during the process of simulative 160 000 km vehicular exhaust aging, which is mainly caused by thermal sintering due to the high temperature of the exhaust gases. Compared to Pt/TiO$_2$, La-modified Pt/TiO$_2$–La$_2$O$_3$ can efficiently reduce Pt particle sintering and maintain a larger Pt surface area to volume ratio under exposure to high-temperature exhaust gases, and hence exhibit better catalytic performance after undergoing simulative 160 000 km vehicular exhaust aging, which is consistent with the results shown in ESI Fig. 3.†

3.3.5 SEM images and surface Pt concentration. In order to investigate whether La doping inhibited the sintering of TiO$_2$-based DOC catalysts during practical use, scanning electron microscopy (SEM) was employed to observe the catalyst morphologies before and after simulative 160 000 km vehicle aging. To get first-hand morphological information on the catalysts in practical use, ceramic honeycombs of the mono-lithic catalysts were cut and then were observed. As shown in Fig. 9, the Pt/TiO$_2$ catalyst exhibits an average particle size of about 2 μm with a few larger particles (5 μm), while for the Pt/TiO$_2$–La$_2$O$_3$ catalyst, the average particle size is about 4 μm with a few smaller particles (1–2 μm); after mimicking 160 000 km of vehicle aging, the particles size of the Pt/TiO$_2$(A) catalyst sharply increased to larger than 10 μm, while the Pt/TiO$_2$–La$_2$O$_3$(A) catalyst still exhibits a particle size of approximately 4 μm. Thus it can be seen that La modification successfully suppressed the sintering of the Pt/TiO$_2$ catalyst particles during long-term application under exposure to high-temperature diesel vehicular exhaust gases, which would reduce the embedding of
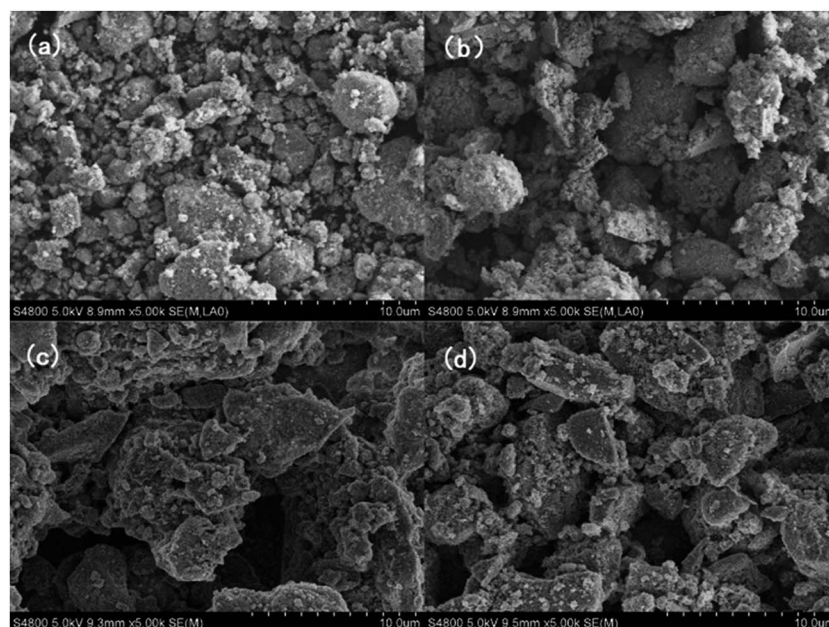

Fig. 9 SEM images of the fresh (a) Pt/TiO$_2$ and (b) Pt/TiO$_2$–La$_2$O$_3$ catalysts and the simulative vehicle-aged (c) Pt/TiO$_2$(A) and (d) Pt/TiO$_2$–La$_2$O$_3$(A) catalysts.

surface Pt species (active component) and hence mitigate the reactivity decrease.

To study the effect of catalyst particle sintering on the embedding of surface Pt particles, X-ray photoelectron spectroscopy (XPS) was carried out and the surface Pt atomic concentrations of the fresh and aged catalysts were estimated using the sensitivity factor method.[53] As shown in ESI Fig. 6,† the Pt (active phase) signal intensity for the fresh samples is obviously stronger than that for the mimicking vehicle-aged samples. The Pt chemical state differences between the fresh Pt/TiO₂ and Pt/TiO₂–La₂O₃ are potentially attributed to the difference in the Pt oxidation degree resulting from the difference in particle size.[17,63] The surface Pt atomic concentrations of the catalysts are listed in Table 6; the surface Pt concentrations of fresh Pt/TiO₂ and Pt/TiO₂–La₂O₃ are 0.87 at% and 0.73 at%, respectively. For the simulative 160 000 km vehicle-aged samples, the surface Pt concentrations of Pt/TiO₂(A) and Pt/TiO₂–La₂O₃(A) are 0.07 at% and 0.27 at%, respectively. It can be seen that the surface Pt (active phase) content of the fresh catalysts is obviously higher than that of the mimicking vehicle-aged samples, mainly because of catalyst surface contamination and support pore structure collapse closing over the surface Pt particles during long-term use.[34,65] In addition, the Pt dispersion of the fresh and 750 °C aged catalysts was measured by CO chemisorption. The Pt dispersions of Pt/TiO₂, Pt/TiO₂–La₂O₃, Pt/TiO₂(750) and Pt/TiO₂–La₂O₃(750) were 22.8%, 35.6%, 7.7% and 15.2%, respectively. It can be seen that after the same aging process, the surface Pt concentration of aged Pt/TiO₂–La₂O₃ is significantly higher than that of aged Pt/TiO₂, which indicates that there are significantly more exposed surface Pt species for aged Pt/TiO₂–La₂O₃ than for Pt/TiO₂. It is thus clear that La modification alleviated Pt/TiO₂–La₂O₃ catalyst surface active component loss during the aging process, and hence contributed to maintaining the excellent reactivity of Pt/TiO₂–La₂O₃ as well as improving the aging resistance. These analysis results show good agreement with the TEM results and catalytic activity results (ESI Fig. 3†).

4. Conclusions

From the above results, it can be concluded that an appropriate dopant amount of lanthana in TiO₂–La₂O₃ composites can maintain the naturally excellent sulfur resistance of TiO₂ and significantly enhance the high-temperature resistibility of TiO₂. Some of the La³⁺ doped ions migrate to the grain boundary of the TiO₂ crystal, which can inhibit the grain growth of TiO₂ by increasing the diffusion barrier at the TiO₂–TiO₂ grain contacts and restricting the direct contact of the grains. Other La³⁺ doped ions replace some of the Ti⁴⁺ ionic sites to form Ti–O–La bands at the interface. The formation of the La³⁺ stabilized Ti–O (Ti–O–La) bonds can defer the anatase-to-rutile phase transition temperature by causing the transfer of electrons from La³⁺ (which is more electropositive) to O²⁻, hence strengthening the bonding between the less electropositive Ti⁴⁺ ions. The stabilization of the TiO₂ crystal structure by the La³⁺ dopant is favorable for maintaining the good texture of the TiO₂–La₂O₃ composite at high temperatures, and consequently restraining

Pt particle agglomeration and surface Pt atom loss. Furthermore, the stabilization of the TiO₂–La₂O₃ texture is beneficial for suppressing the catalyst particle sintering of Pt/TiO₂–La₂O₃ at high temperatures, meaning that the as-prepared Pt/TiO₂–La₂O₃ catalyst still exhibits superior activity even after different high-temperature aging processes. The catalytic performance of the La₂O₃-modified Pt/TiO₂–La₂O₃ catalyst for the purification of diesel exhaust gases (CO and C₃H₆) is almost not reduced after thermal treatment at 750 °C; however, the reactivity of the Pt/TiO₂ catalyst is reduced by about 40% after the 750 °C treatment. Additionally, the 850 °C thermally treated catalysts and simulative 160 000 km vehicle-aged samples also show the same trend; lanthana modification obviously enhanced the high-temperature resistance of the Pt/TiO₂ catalyst. Thus, this work demonstrates that lanthana-modified Pt/TiO₂–La₂O₃ DOC catalysts display excellent high-temperature thermal stability and efficiently maintain the naturally outstanding sulfur resistance of TiO₂-based catalysts, which is beneficial for practical applications.

Acknowledgements

References

1 D. Fino, S. Bensaid, M. Piumetti and N. Russo, A review on the catalytic combustion of soot in Diesel particulate filters for automotive applications: From powder catalysts to structured reactors, *Appl. Catal., A*, 2016, **509**, 75–96.

2 C. Liu, J.-W. Shi, C. Gao and C. Niu, Manganese oxide-based catalysts for low-temperature selective catalytic reduction of NO$_x$ with NH₃: A review, *Appl. Catal., A*, 2016, **522**, 54–69.

3 T. Johnson, *Review of Vehicular Emissions Trends*, SAE Technical Paper, 2015-01-0993, 2015.

4 T. Johnson, *Vehicular Emissions in Review*, SAE Technical Paper, 2014-01-1491, 2014.

5 A. K. Wu, X. D. Yang, H. Zhou and K. J. Lu, Applied Mechanics and Materials, *Study on the Effect of Fuel Sulfur Content on Emission Characteristics in Diesel Engine*, Trans Tech Publ, 2014, pp. 27–30.

6 Z.-Z. Yang, Y. Yang, M. Zhao, M.-C. Gong and Y.-Q. Chen, Enhanced Sulfur Resistance of Pt–Pd/CeO₂–ZrO₂–Al₂O₃ Commercial Diesel Oxidation Catalyst by SiO₂ Surface Cladding, *Acta Phys.-Chim. Sin.*, 2014, **30**, 1187–1193.

7 H. N. Sharma, S. L. Suib and A. B. Mhadeshwar, Interactions of Sulfur Oxides with Diesel Oxidation Catalysts (DOCs),

Novel Materials for Catalysis and Fuels Processing, Oxford University Press, USA, 2013, vol. 1132, pp. 117–155.

8 K. Zhang, J. Hu, S. Gao, Y. Liu, X. Huang and X. Bao, Sulfur content of gasoline and diesel fuels in northern China, *Energy Policy*, 2010, **38**, 2934–2940.

9 P.-Q. Tan, Z.-Y. Hu and D.-M. Lou, Regulated and unregulated emissions from a light-duty diesel engine with different sulfur content fuels, *Fuel*, 2009, **88**, 1086–1091.

10 J. Li, A. Kumar, X. Chen, N. Currier and A. Yezerets, *Impact of Different Forms of Sulfur Poisoning on Diesel Oxidation Catalyst Performance*, SAE Technical Paper, 2013-01-0514, 2013.

11 J.-Y. Luo, D. Kisinger, A. Abedi and W. S. Epling, Sulfur release from a model Pt/Al$_2$O$_3$ diesel oxidation catalyst: Temperature-programmed and step-response techniques characterization, *Appl. Catal., A*, 2010, **383**, 182–191.

12 Y. Kanno, T. Hihara, T. Watanabe and K. Katoh, *Low Sulfate Generation Diesel Oxidation Catalyst*, SAE Technical Paper, 2004-01-1427, 2004.

13 J. Li, Y. Zhu, R. Ke and J. Hao, Improvement of catalytic activity and sulfur-resistance of Ag/TiO$_2$–Al$_2$O$_3$ for NO reduction with propene under lean burn conditions, *Appl. Catal., B*, 2008, **80**, 202–213.

14 H. Hirata, I. Hachisuka, Y. Ikeda, S. Tsuji and S. i. Matsumoto, NO$_x$ storage-reduction three-way catalyst with improved sulfur tolerance, *Top. Catal.*, 2001, **16**, 145–149.

15 U. Hideaki, *Development of Catalyst for Diesel Engine*, SAE Technical Paper, 980195, 1998.

16 Z. Yang, J. Li, H. Zhang, Y. Yang, M. Gong and Y. Chen, Size-dependent CO and propylene oxidation activities of platinum nanoparticles on the monolithic Pt/TiO$_2$–YO$_x$ diesel oxidation catalyst under simulative diesel exhaust conditions, *Catal. Sci. Technol.*, 2015, **5**, 2358–2365.

17 Z. Yang, N. Zhang, Y. Cao, M. Gong, M. Zhao and Y. Chen, Effect of yttria in Pt/TiO$_2$ on sulfur resistance diesel oxidation catalysts: enhancement of low-temperature activity and stability, *Catal. Sci. Technol.*, 2014, **4**, 3032–3043.

18 Z. Yang, Y. Chen, M. Zhao, J. Zhou, M. Gong and Y. Chen, Preparation and Properties of Pt/Zr$_x$Ti$_{1-x}$O$_2$ Catalysts with Low-Level SO$_2$ Oxidation Activity for Diesel Oxidation, *Chin. J. Catal.*, 2012, **33**, 819–826.

19 J. Yang, S. Mei and J. M. Ferreira, Hydrothermal synthesis of nanosized titania powders: influence of peptization and peptizing agents on the crystalline phases and phase transitions, *J. Am. Ceram. Soc.*, 2000, **83**, 1361–1368.

20 J. F. Porter, Y.-G. Li and C. K. Chan, The effect of calcination on the microstructural characteristics and photoreactivity of Degussa P-25 TiO$_2$, *J. Mater. Sci.*, 1999, **34**, 1523–1531.

21 G. Cavataio, H.-W. Jen, J. W. Girard, D. Dobson, J. R. Warner and C. K. Lambert, *Impact and prevention of ultra-low contamination of platinum group metals on SCR catalysts due to DOC design*, SAE Technical Paper, 2009-01-0627, 2009.

22 A. Bueno-López, I. Such-Basáñez and C. Salinas-Martínez de Lecea, Stabilization of active Rh$_2$O$_3$ species for catalytic decomposition of N$_2$O on La-, Pr-doped CeO$_2$, *J. Catal.*, 2006, **244**, 102–112.

23 P. Jiang, G. Lu, Y. Li, Y. Guo, Y. Guo and X. Wang, Preparation of La$_2$O$_3$-doped CeO$_2$–ZrO$_2$ Solid Solution with High Thermal Stability by Water-in-Oil Microemulsion, *Chem. Lett.*, 2004, **33**, 1064–1065.

24 R. Strobel, S. E. Pratsinis and A. Baiker, Flame-made Pd/La$_2$O$_3$/Al$_2$O$_3$ nanoparticles: thermal stability and catalytic behavior in methane combustion, *J. Mater. Chem.*, 2005, **15**, 605–610.

25 T. Yamamoto, T. Hatsui, T. Matsuyama, T. Tanaka and T. Funabiki, Structures and Acid-Base Properties of La/Al$_2$O$_3$ Role of La Addition to Enhance Thermal Stability of γ-Al$_2$O$_3$, *Chem. Mater.*, 2003, **15**, 4830–4840.

26 Y.-T. Ma and S.-D. Li, Photocatalytic Activity of TiO$_2$ Nanofibers with Doped La Prepared by Electrospinning Method, *J. Chin. Chem. Soc.*, 2015, **62**, 380–384.

27 X.-M. Chen, Z.-J. Liu, J.-T. Tang, C.-L. Teng, T.-J. Cai and Q. Deng, La-modified mesoporous TiO$_2$ nanoparticles with enhanced photocatalytic activity for elimination of VOCs, *J. Porous Mater.*, 2015, **22**, 361–367.

28 Y. Cong, B. Tian and J. Zhang, Improving the thermal stability and photocatalytic activity of nanosized titanium dioxide *via* La^{3+} and N co-doping, *Appl. Catal., B*, 2011, **101**, 376–381.

29 R. Gopalan and Y. S. Lin, Evolution of Pore and Phase Structure of Sol–Gel Derived Lanthana Doped Titania at High Temperatures, *Ind. Eng. Chem. Res.*, 1995, **34**, 1189–1195.

30 C. P. Sibu, S. R. Kumar, P. Mukundan and K. G. K. Warrier, Structural Modifications and Associated Properties of Lanthanum Oxide Doped Sol–Gel Nanosized Titanium Oxide, *Chem. Mater.*, 2002, **14**, 2876–2881.

31 B. M. Reddy, P. M. Sreekanth, E. P. Reddy, Y. Yamada, Q. Xu, H. Sakurai and T. Kobayashi, Surface Characterization of La$_2$O$_3$–TiO$_2$ and V$_2$O$_5$/La$_2$O$_3$–TiO$_2$ Catalysts, *J. Phys. Chem. B*, 2002, **106**, 5695–5700.

32 M. Aubert, T. Birchem and G. Blanchard, Composition based on cerium oxide and on zirconium oxide with a high specific surface and a high oxygen storage capacity, process of preparation and use in catalysts, *US Pat.*, 6,228,799, 2001.

33 O. Larcher and E. Rohart, Composition based on cerium oxide and on zirconium oxide having a high reducibility and high specific surface, methods for the preparation thereof and use as a catalyst, *US Pat.*, 8,192,710, 2012.

34 J. Andersson, M. Antonsson, L. Eurenius, E. Olsson and M. Skoglundh, Deactivation of diesel oxidation catalysts: Vehicle- and synthetic aging correlations, *Appl. Catal., B*, 2007, **72**, 71–81.

35 J. Kašpar, P. Fornasiero and N. Hickey, Automotive catalytic converters: current status and some perspectives, *Catal. Today*, 2003, **77**, 419–449.

36 M. M. Koranne and J. N. Pryor, Sulfur tolerant alumina catalyst support, *US Pat.*, 8158257, 2012.

37 K. Foger and J. R. Anderson, Temperature programmed desorption of carbon monoxide adsorbed on supported platinum catalysts, *Appl. Surf. Sci.*, 1979, **2**, 335–351.

38 H. Ueno, T. Furutani, T. Nagami, N. Aono, H. Goshima and K. Kasahara, *Development of catalyst for diesel engine*, SAE Technical Paper, 980195, 1998.

39 S. E. Voltz, C. R. Morgan, D. Liederman and S. M. Jacob, Kinetic Study of Carbon Monoxide and Propylene Oxidation on Platinum Catalysts, *Ind. Eng. Chem. Prod. Res. Dev.*, 1973, **12**, 294–301.

40 J. M. G. Amores and V. S. Escribano, Anatase crystal growth and phase transformation to rutile in high-area TiO_2, MoO_3–TiO_2 and other TiO_2-supported oxide catalytic systems, *J. Mater. Chem.*, 1995, **5**, 1245–1249.

41 R. C. Weast and M. J. Astle, *Handbook of Chemistry and Physics*, CRC Press, Boca Raton, FL, 59th edn, 1978.

42 X.-Z. Ding and X.-H. Liu, Correlation Between Anatase-to-rutile Transformation and Grain Growth in Nanocrystalline Titania Powders, *J. Mater. Res.*, 1998, **13**, 2556–2559.

43 X. Quan, H. Tan, Q. Zhao and X. Sang, Preparation of lanthanum-doped TiO_2 photocatalysts by coprecipitation, *J. Mater. Sci.*, 2007, **42**, 6287–6296.

44 K. M. Parida and N. Sahu, Visible light induced photocatalytic activity of rare earth titania nanocomposites, *J. Mol. Catal. A: Chem.*, 2008, **287**, 151–158.

45 K. B. Jaimy, S. Ghosh and K. Gopakumar Warrier, Enhanced visible light activity of nano-titanium dioxide doped with multiple ions: Effect of crystal defects, *J. Solid State Chem.*, 2012, **196**, 465–470.

46 B. M. Reddy, B. Chowdhury and P. G. Smirniotis, An XPS study of La_2O_3 and In_2O_3 influence on the physicochemical properties of MoO_3/TiO_2 catalysts, *Appl. Catal., A*, 2001, **219**, 53–60.

47 D. Xu, L. Feng and A. Lei, Characterizations of lanthanum trivalent ions/TiO_2 nanopowders catalysis prepared by plasma spray, *J. Colloid Interface Sci.*, 2009, **329**, 395–403.

48 D. R. Sellick, A. Aranda, T. García, J. M. López, B. Solsona, A. M. Mastral, D. J. Morgan, A. F. Carley and S. H. Taylor, Influence of the preparation method on the activity of ceria zirconia mixed oxides for naphthalene total oxidation, *Appl. Catal., B*, 2013, **132–133**, 98–106.

49 Y. Yang, Z.-Z. Yang, H.-D. Xu, B.-Q. Xu, Y.-H. Zhang, M.-C. Gong and Y.-Q. Chen, Influence of La on CeO_2–ZrO_2 Catalyst for Oxidation of Soluble Organic Fraction from Diesel Exhaust, *Acta Phys.-Chim. Sin.*, 2015, **31**, 2358–2365.

50 A. Galtayries, R. Sporken, J. Riga, G. Blanchard and R. Caudano, XPS comparative study of ceria/zirconia mixed oxides: powders and thin film characterisation, *J. Electron Spectrosc. Relat. Phenom.*, 1998, **88–91**, 951–956.

51 Z. Nie, T. Zuo, M. Zhou, Y. Wang, J. Wang and J. Zhang, High Temperature XPS/AES Investigation of Mo–La_2O_3 Cathode I. Species and Properties of Oxygen on Surface, *J. Chin. Soc. Rare Earths*, 1999, **17**, 135–139.

52 J. Wang, Z. Nie, M. Zhou, J. Zhang, Y. Hu and T. Zuo, A Study of Chemical Stability of La_2O_3 in Carburized La_2O_3–Mo Cathode Materials, *Chin. Rare Earths*, 2000, **21**, 18–21.

53 C. D. Wagner, W. M. Riggs, J. F. Moulder and G. E. Muilenberg, *Handbook of X-Ray Photoelectron Spectroscopy*, Perkin-Elmer Corporation, Minnesota, 1979.

54 M. Thommes, Physical adsorption characterization of nanoporous materials, *Chem.-Ing.-Tech.*, 2010, **82**, 1059–1073.

55 G. Leofanti, M. Padovan, G. Tozzola and B. Venturelli, Surface area and pore texture of catalysts, *Catal. Today*, 1998, **41**, 207–219.

56 M. Aubert, T. Birchem, G. Blanchard and O. Touret, Composition based on zirconium oxide and cerium oxide, preparation method therefor and use thereof, *US Pat.*, 6,214,306, 2001.

57 C. Hedouin, Process for preparing an oxide based on zirconium and titanium, oxides obtained thereby, and use of said oxides as catalysts, *US Pat.*, 7,524,474, 2009.

58 J. A. Hunns, M. Arroyo, A. F. Lee, J. M. Escola, D. Serrano and K. Wilson, Hierarchical mesoporous Pd/ZSM-5 for the selective catalytic hydrodeoxygenation of *m*-cresol to methylcyclohexane, *Catal. Sci. Technol.*, 2016, **6**, 2560–2564.

59 P. S. F. Mendes, G. Lapisardi, C. Bouchy, M. Rivallan, J. M. Silva and M. F. Ribeiro, Hydrogenating activity of Pt/zeolite catalysts focusing acid support and metal dispersion influence, *Appl. Catal., A*, 2015, **504**, 17–28.

60 T. Wu, Q. Zhang, W. Cai, P. Zhang, X. Song, Z. Sun and L. Gao, Phyllosilicate evolved hierarchical Ni- and Cu–Ni/SiO_2 nanocomposites for methane dry reforming catalysis, *Appl. Catal., A*, 2015, **503**, 94–102.

61 R. Portela, V. E. Garcia-Sanchez, M. Villarroel, S. B. Rasmussen and P. Avila, Influence of the pore generation method on the metal dispersion and oxidation activity of supported Pt in monolithic catalysts, *Appl. Catal., A*, 2016, **510**, 49–56.

62 C. Chen, F. Chen, L. Zhang, S. Pan, C. Bian, X. Zheng, X. Meng and F.-S. Xiao, Importance of platinum particle size for complete oxidation of toluene over Pt/ZSM-5 catalysts, *Chem. Commun.*, 2015, **51**, 5936–5938.

63 A. Boubnov, S. Dahl, E. Johnson, A. P. Molina, S. B. Simonsen, F. M. Cano, S. Helveg, L. J. Lemus-Yegres and J.-D. Grunwaldt, Structure–activity relationships of Pt/Al_2O_3 catalysts for CO and NO oxidation at diesel exhaust conditions, *Appl. Catal., B*, 2012, **126**, 315–325.

64 S. Bonanni, K. Ait-Mansour, W. Harbich and H. Brune, Reaction-Induced Cluster Ripening and Initial Size-Dependent Reaction Rates for CO Oxidation on Pt_n/$TiO_2(110)$–(1*x*1), *J. Am. Chem. Soc.*, 2014, **136**, 8702–8707.

65 A. Winkler, D. Ferri and M. Aguirre, The influence of chemical and thermal aging on the catalytic activity of a monolithic diesel oxidation catalyst, *Appl. Catal., B*, 2009, **93**, 177–184.